THE JOURNAL OF PHYSICAL CHEMISTRY C

Article

pubs.acs.org/JPCC

DFT Modeling of the Adsorption of Trimethylphosphine Oxide at the Internal and External Surfaces of Zeolite MFI

Carlos E. Hernandez-Tamargo,[†,‡] Alberto Roldan,[‡] and Nora H. de Leeuw*[,†,‡]

[†]Department of Chemistry, University College London, 20 Gordon Street, London, United Kingdom WC1H 0AJ

[‡]School of Chemistry, Cardiff University, Main Building, Park Place, Cardiff, United Kingdom CF10 3AT

ABSTRACT: The characterization of the acidity of zeolites allows a direct correlation with their catalytic activity. To this end, probe molecules are utilized to obtain a ranking of acid strengths. Trimethylphosphine oxide (TMPO) is a widely used probe molecule, which allows the sensing of solid acids by using ^{31}P NMR. We have performed calculations based on the density functional theory to investigate the Brønsted acid (BA) sites in zeolite MFI by adsorbing TMPO as a probe molecule. We have considered the substitution of silicon at the T2 site by aluminum, both at the internal cavity and at the external surface. The different acid strengths observed in the zeolite MFI when probed by TMPO (very strong, strong, and weak) may depend on the basicity of the centers sharing the acid proton. If the proton lies between the TMPO and one of the framework oxygen atoms binding the Al, the acidity is strong. When the framework oxygen atom is not directly binding the Al, it is less basic and a shortening of the TMPO−H distance is observed, causing an acid response of very strong. Finally, if two TMPO molecules share the proton, the TMPO−H distance elongates, rendering a weak acid character.

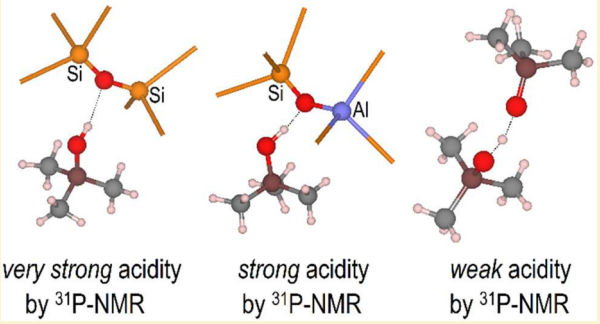

1. INTRODUCTION

Zeolites are well-known microporous materials whose frameworks are formed by corner-sharing SiO_4 tetrahedra. A negative charge is created when Al^{3+} substitutes Si^{4+} at the center of a tetrahedron, which is compensated by extraframework cations within the pore system of the zeolite. Brønsted acid (BA) sites are generated when the counterbalancing cation is a proton that covalently binds the O atom bridging the Al and the Si.[1] These BA sites, together with the size selectivity of the pore system, are the driving forces behind the wide range of catalytic applications of zeolites.[2−5]

The characterization of the zeolite's acidity by number, density, and strength may allow a direct correlation to its catalytic activity. However, in contrast with an acid in an aqueous medium, there is no unique way to rank the acidity of solid materials.[6] In zeolites, the proficiency of each BA as a proton donor will depend on its location within the pore system and its accessibility by the adsorbed reactant,[6] which hinders the analysis of the zeolite's acidity.

The strength and number of the BA sites are usually measured through the adsorption of probe molecules, which act as bases and are protonated upon interaction with the BA sites. There are several analytical methods to evaluate the extent of the protonation of the probe molecule,[1,6] for example, the nuclear magnetic resonance (NMR), which provides high accuracy and specificity to examine the consequences of the proton transfer.[7] The movement of the acid proton from the BA site to the probe molecule may be sensed directly when recording the ^{1}H NMR spectrum, as in the case of the pyridine/pyridinium system.[8] In addition, other nuclei different from ^{1}H may also be analyzed if their magnetic response to the applied field is affected by the protonation of the probe molecule, e.g., ^{13}C in acetone[9] and ^{31}P in trimethylphosphine oxide.[10]

Trimethylphosphine oxide (TMPO, see Figure 1 for a representation of the molecule's structure) has shown to be a suitable molecule for sensing BA sites of different strength, owing to the high sensibility of the TMPO's ^{31}P nucleus to the intensity of the phosphine−BA interaction.[7] The ^{31}P chemical shift moves from 39 ppm (crystalline TMPO) toward a range of 50−105 ppm upon protonation of the TMPO's oxygen atom; the stronger the proton transfer, the larger the chemical shift.[7] Therefore, the strength of BA sites in zeolites can be classified according to the value of the ^{31}P chemical shift as very strong (90−80 ppm), strong (80−70 ppm), and weak (70−60 ppm), where 86 ppm is the calculated threshold of superacidity for TMPO.[7,10−12]

The present work proposes a density functional theory (DFT) study of the adsorption of TMPO in zeolite MFI. Zeolite Socony Mobil-5 (ZSM-5) has the framework type of MFI, which is a material with a wide array of industrial applications and high versatility.[13−16] We have described in detail the TMPO−BA interaction at the internal and external surfaces of zeolite MFI, providing atomic level information to

Received: April 5, 2016
Revised: August 4, 2016
Published: August 8, 2016

DOI: 10.1021/acs.jpcc.6b03448
J. Phys. Chem. C 2016, 120, 19097−19106

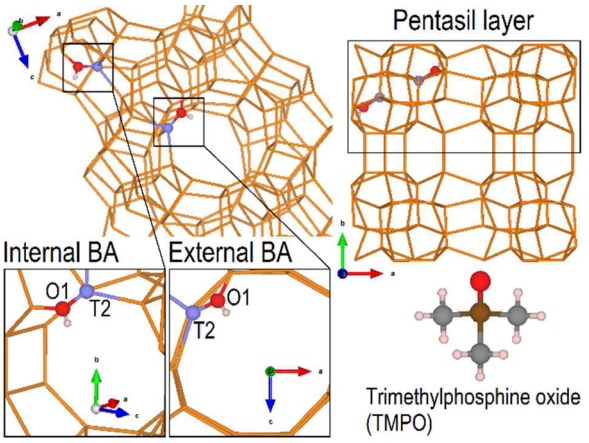

Figure 1. Representation of the BA sites at the internal (bottom, left panel) and at the external (bottom, right panel) surfaces. One of the two pentasil layers that form the slab is identified by a black-line rectangle (top, right panel). The Al-substituted T2-site (light blue ball) with the proton (white ball) at the O1 position (red ball) are shown. The rest of the O atoms and silanol OH groups were deleted for a better view; Si atoms are represented by orange sticks. A molecule of trimethylphosphine oxide is shown in the bottom-right corner; H is represented in white, C in gray, P in brown, and O in red.

complement previous experimental reports. The MFI's internal and external surfaces behave differently: three types of BA sites of variable strength have been detected at the internal surface (very strong, strong, and weak), whereas the strong BA sites tend to disappear at the external surface.[10,12] Thus, to distinguish between these sites, alternative experimental methods must be used. For instance, silica chemical vapor deposition (Si-CVD) deactivates the external surface while keeping the internal sites undamaged,[10] whereas the inclusion of tributylphosphine oxide (TBPO), which is too big to diffuse into the zeolite's pore system, allows the exclusive sensing of the external surface.[10,12]

We have also explored how a variable number of TMPO molecules affects the acid response of the BA site. Zheng et al. have previously reported the enhancement of the Brønsted acidity in mordenite by the intermolecular solvent effect when several TMPO molecules are confined in the micropore.[17] The authors relate this effect to van der Waals interactions among the TMPO molecules, which provoke simultaneous decrease and increase of the O−H distance of the TMPO molecules, generating in consequence superacidity and weak acidity, respectively.[6,7,17]

2. COMPUTATIONAL METHODS

The results presented in this work were obtained using the DFT approximation as implemented in the Vienna Ab-initio Simulation Package (VASP).[18−21] The generalized gradient approximation (GGA) under the scheme proposed by Perdew, Burke, and Ernzerhof (PBE) was used in all calculations.[22] Grimme's method of the sum of pairs was added to the GGA energy to account for the long-range-interactions (DFT-D2).[23] The inclusion of dispersion corrections improves the predicted cell parameters and elastic properties of the zeolite MFI.[24] The valence electrons were treated explicitly using a basis set of plane waves, although their nodal features and interactions with the ion were included within the projected-augmented-wave method (PAW).[25,26] The number of plane waves considered during the calculations was determined by a maximum kinetic energy of 500 eV. The electronic convergence was improved using the Gaussian smearing method with a bandwidth of 0.1 eV for the zeolite and zeolite−TMPO systems and 0.01 eV for the isolated TMPO molecule.[27,28] Only the Gamma point was taken into account during the numerical integration over the Brillouin zone due to the large dimensions of the MFI unit cell. Finally, the electronic threshold was set to 10^{-5} eV.

The orthorhombic unit cell of the MFI framework has 12 nonequivalent T-sites to be substituted by Al (the center of each tetrahedron is referred as T-site and numbered according to the symmetry of the zeolite's unit cell). In conjunction, the acid proton can bind four O atoms for each T-site, which produces a high number of possible combinations, making practically impossible a detailed analysis of each arrangement. We have therefore opted for Al substitution in the T2-site, binding the proton to O1 (see Figure 1), which allowed us to focus on the acid response of that BA site to the number and orientation of TMPO molecules, as well as the consequences of the BA site location at the internal or the external surface.

The T2-site was chosen for the Al substitution, and the charge-compensating proton was bound to the O1 atom, leading to the formation of the BA site (see Figure 1). This specific position was chosen because T2 is at the interception of straight and sinusoidal channels and is easily accessible by the probe molecule, allowing a fair study of the TMPO agglomeration around the acid site. We have studied the proton transfer to TMPO, accommodating up to three molecules simultaneously. The optimized cell parameters of the zeolite MFI were 20.317, 19.979, and 13.413 Å along the *a*, *b*, and *c* directions, respectively,[24] within 1% of the experimental measurements.[29] Using periodic boundary conditions, the external surface was described by a slab formed of two pentasil layers,[30] as shown in Figure 1, with a surface area per unit cell of 272.512 $Å^2$ and a perpendicular vacuum gap of 20 Å between the slabs. In this termination, each dangling Si−O bond was properly saturated by hydroxyl, thus forming silanol groups at the bottom and top surfaces of the slab; in the case of pentasil layers, there is only one dangling Si−O bond per Si atom.[24] The isolated TMPO molecule was first optimized in a 20 × 21 × 22 $Å^3$ cell, before it was loaded in the zeolite, varying its numbers and orientations, ahead of a full geometry optimization.

The initial geometries set for optimization were constructed by loading the TMPO molecules in close proximity to the acid proton of the zeolite. These geometries were locally optimized using a conjugate gradient algorithm until all forces acting on the ions were smaller than 0.03 eV/Å. The local relaxations were followed by short quantum molecular dynamics (MD) simulations over a simulation time of 10 ps, with a time step of 0.5 fs. A microcanonical ensemble was used for each geometry during the first 2.5 ps of MD while keeping the temperature at 300 K. A canonical ensemble centered at 300 K was simulated during the next 7.5 ps of MD, controlling the temperature fluctuation with a Nosé thermostat.[31−33] We have used the last 2.5 ps to obtain the average structural parameters of interest.

All the images related to structural and charge density visualizations were obtained with the code Visualization for Electronic and Structural Analysis (VESTA 3).[34]

2.1. Classification of the Acid Strength. Brønsted acid sites of different strength are detected in zeolite MFI when probed with TMPO. According to Seo et al., the acid strength can be classified as very strong (86 ppm), strong (76 ppm), and weak (68 and 66 ppm),[12] in agreement with previous

DOI: 10.1021/acs.jpcc.6b03448
J. Phys. Chem. C 2016, 120, 19097−19106

experimental reports.[10] Zheng et al. reproduced the range of ^{31}P chemical shifts by modeling the adsorption of TMPO on zeolite MFI, which was represented by a cluster of eight T-sites.[11] The authors tuned the acid strength by varying the terminal Si−H distances of the cluster, thus controlling the extent of the proton transfer from the BA site to the TMPO's oxygen atom, hereafter referred to as $O_{(P)}$. Zheng et al. reported a wide spectrum of $O_{(P)}$−H distances after optimization, calculating the ^{31}P chemical shift for each geometry; those distances ranged from 1.368 Å (45.5 ppm) to 1.014 Å (88.9 ppm).[11]

We noted that our calculated $O_{(P)}$−H distances changed within the limits proposed by Zheng et al., and hence we assumed that the theoretical work in ref 11 matches the expected ^{31}P chemical shift for our own data. Figure 2 shows

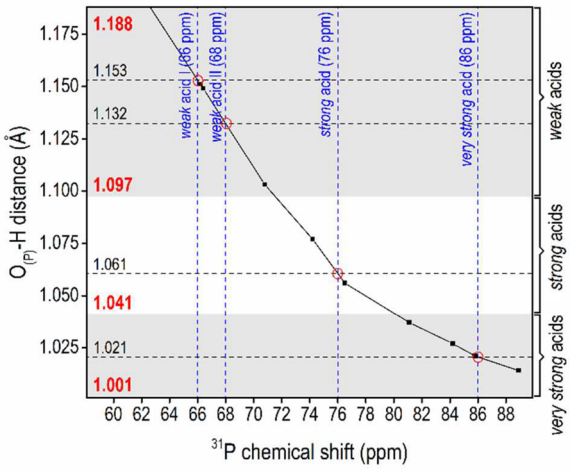

Figure 2. Correlation of the $O_{(P)}$−H distances and the ^{31}P chemical shifts using Zheng et al. data (black squares linked with black lines).[11] The experimental classification of the acid sites of the zeolite MFI according to the TMPO ^{31}P chemical shift is indicated by vertical dashed blue lines.[10,12] The experimental classification is used to extrapolate the expected $O_{(P)}$−H distances from its interception with the theoretical curve (indicated by red circles); the corresponding distance values are written above the horizontal dashed black lines. The spectrum of $O_{(P)}$−H distances is divided into three zones taking the middle points between the extrapolated $O_{(P)}$−H distances. These zones are shaded alternately in light gray and white, corresponding to (top) weak acids, (center) strong acids, and (bottom) very strong acids; the limits of each range are indicated by the red numbers at the left-hand side of the graph.

the correlation between the $O_{(P)}$−H distance and the ^{31}P chemical shift as calculated in ref 11. From that curve, we extrapolated the $O_{(P)}$−H distances corresponding to the experimental measurement of the ^{31}P chemical shift that classifies the BA sites by strength (see Figure 2).[12] Taking the middle points between the extrapolated $O_{(P)}$−H distances, we obtained approximate ranges of $O_{(P)}$−H distances to classify the effective acid strength of our model (see Figure 2). The ranges are as follows: very strong acid (from 1.001 to 1.041 Å), strong acid (from 1.041 to 1.097 Å), and weak acid (from 1.097 to 1.188 Å). In comparison, we calculated a $O_{(P)}$−H distance of 0.978 Å for a fully protonated TMPO molecule loaded in the zeolite, for which the position of the P atom was fixed at the center of the pore interception of zeolite MFI to avoid any H-bonding with nearby framework O atoms. In addition, on the basis of Car−Parrinello MD of a hydronium ion in aqueous medium, Tuckerman et al. have reported an O−H distance of 1.3 Å for the shared proton between two H_2O molecules in the complex $(H_5O_2)^+$.[35]

3. RESULTS AND DISCUSSION

3.1. Adsorption of One TMPO Molecule. In this section we have presented the adsorption of a single TMPO molecule in close proximity to the BA proton. The TMPO was adsorbed on the internal and external surfaces of the zeolite by placing the $O_{(P)}$ atom at 2.0 Å from the acidic proton. Two different orientations of the TMPO molecule with respect to the BA proton were tested, varying the values of the P−$O_{(P)}$−H and $O_{(P)}$−H−$O1_{(Al)}$ angles (the label $O1_{(Al)}$ refers to the framework O atom binding simultaneously the Al atom and the acidic proton; in the present case, position O1).

During the local relaxations, the proton was transferred from the BA site to the TMPO molecule, at both the internal and external surfaces, regardless of the initial configuration. The Bader analysis of atomic charges[36−38] confirmed the movement of the proton; the total charge obtained for protonated phosphine oxides ranged from +0.8 to 0.9 e^-, and more than 80% of the corresponding negative charge left in the zeolite framework was associated with the AlO_4 tetrahedron. Figure 3

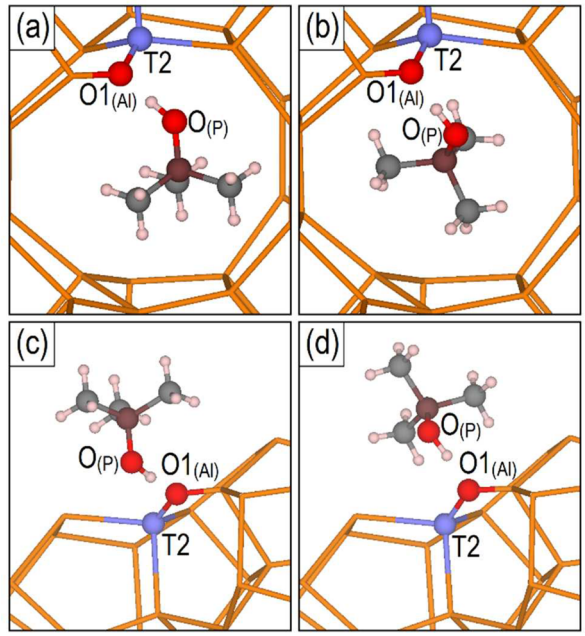

Figure 3. Representation of the interaction of a single TMPO molecule with (a, b) the internal and (c, d) the external BA sites after local optimization; H in white, C in gray, P in brown, O in red, Al in light blue, and Si represented by orange sticks. All the framework O atoms (except the protonated one) and silanol OH groups were deleted for an enhanced view. Related structural values are presented in Table 1.

shows the final equilibrium structures with the corresponding structural parameters listed in Table 1. The $O_{(P)}$−H bond length ranged from 1.045 to 1.066 Å, i.e., larger than in the MFI external silanol groups (<0.970 Å) and MFI acidic protons with intraframework H-bonds (<1.014 Å).[24] These longer bonds were due to strong H-bonds established between the protonated TMPO molecules and the $O_{(Al)}$ atoms of the framework, with $O_{(P)}$−$O_{(Al)}$ distances below 2.6 Å and H−$O_{(Al)}$−$O_{(P)}$ angles smaller than 3°.[39] According to the division

DOI: 10.1021/acs.jpcc.6b03448
J. Phys. Chem. C 2016, 120, 19097−19106

Table 1. Relevant Interatomic Distances (Å) of the 1TMPO/1BA Configurations Shown in Figure 3a−d after Local Optimization

	internal BA		external BA	
	Figure 3a[a]	Figure 3b	Figure 3c	Figure 3d
$O_{(P)}$−H	1.060 (2.000)	1.045 (2.000)	1.066 (2.000)	1.060 (2.000)
$O_{(Al)}$−H	1.459 (0.975)	1.483 (0.975)	1.429 (0.975)	1.465 (0.975)
$O_{(P)}$−$O_{(Al)}$	2.518 (2.975)	2.526 (2.225)	2.492 (2.975)	2.522 (2.225)
P−$O_{(P)}$[b]	1.556	1.561	1.556	1.556

[a]The values before the structural optimization are presented within parentheses. [b]The optimized P−$O_{(P)}$ distance in gas phase is 1.494 Å.

of the spectrum of possible $O_{(P)}$−H distances, shown in Figure 2, the acid strength of the BA site may be classified as *strong* for the four different configurations after local optimization. No evidence of very strong or weak acidity was obtained at this stage. The variation of the adsorption energy could not be correlated with corresponding changes in the $O_{(P)}$−H distance. Nonetheless, the average TMPO interaction energy was larger for the internal BA when compared with the external BA: −190 and −167 kJ/mol, respectively. The contribution of dispersion forces to the total adsorption energy was 47% and 38% for the internal and external BA site, respectively. However, these percentages should be viewed with reservation because the DFT-D2 method tends to overestimate attractive interactions owing to the omission of terms above the two-body contribution; the error can increase beyond 10% for supramolecular complexes.[40]

The MD simulation did not result in significant changes when compared to the local optimization; Table 2 shows the

Table 2. Relevant Interatomic Distances (Å) after 10 ps of MD Simulation Taking the 1TMPO/1BA Configurations Shown in Figure 3a−d as Input Geometries

	internal BA		external BA	
	Figure 3a[a]	Figure 3b	Figure 3c	Figure 3d
$O_{(P)}$−H	1.06 ± 0.05	1.05 ± 0.05	1.08 ± 0.08	1.07 ± 0.06
$O_{(Al)}$−H	1.5 ± 0.1	1.6 ± 0.2	1.5 ± 0.1	1.5 ± 0.1
$O_{(P)}$−$O_{(Al)}$	2.51 ± 0.09	2.6 ± 0.1	2.53 ± 0.09	2.53 ± 0.09
P−$O_{(P)}$	1.56 ± 0.03	1.57 ± 0.03	1.57 ± 0.04	1.57 ± 0.03

[a]Average and standard deviation over the last 2.5 ps of MD simulation.

average values and the standard deviations of the last 2.5 ps. The average values of the $O_{(P)}$−H bond length remained within the range 1.05−1.08 Å, with fluctuations between 0.05 and 0.08 Å, which confirms that the strength of the modeled BA site can only be classified as strong when a single TMPO is adsorbed. Furthermore, we observed the replacement of $O1_{(Al)}$ by $O2_{(Al)}$ as the acceptor of the H-bond for the configuration in Figure 3b (see Figure 4 for a representation of the structure after 10 ps of MD). This movement occurred during the first 2.5 ps of MD simulation, although the acid response continued to be strong.

3.2. Adsorption of Two TMPO Molecules. We next adsorbed two TMPO molecules at a short distance from the BA site to analyze their effect on the proton transfer. Figure 5 shows the most stable structures after local optimization, out of several tested configurations at the internal and external BA sites; related structural parameters are compiled in Table 3. The $O_{(P)}$−H bond length of the configurations in Figure 5 decreased to 1.016 and 1.033 Å for the internal and external surfaces, respectively, suggesting an apparent stronger acidity triggered by the presence of the second TMPO molecule. In

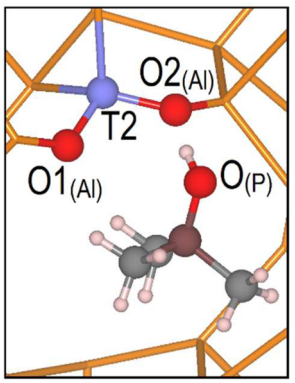

Figure 4. Configuration after 10 ps of MD simulation of the locally optimized structure in Figure 3b.

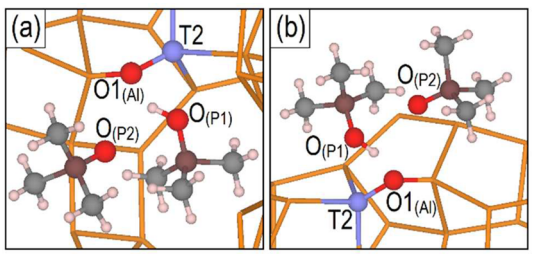

Figure 5. Representation of the adsorption of two TMPO molecules on (a) the internal and (b) the external BA sites after local optimization. H in white, C in gray, P in brown, O in red, Al in light blue, and Si represented by orange sticks. All the framework O atoms (except the protonated one) and silanol OH groups were deleted for an enhanced view. Related structural values are presented in Table 3.

consequence, the acid strength of the internal and external acid sites can be classified as very strong according to the scheme in Figure 2.

We have calculated average adsorption energies per TMPO of −125 kJ/mol for the internal surface and −112 kJ/mol for the external surface, with the dispersion forces representing 84% and 54% of the total adsorption energy, respectively, indicating that the role of van der Waals interactions increases with the number of probe molecules.

The second TMPO is a source of steric hindrance that affects the interaction through H-bonding between the first TMPO and the BA site. Because the protonated TMPO cannot form an ideal orientation in front of the bridging O atom, the H-bond is not strong enough, which produces a further shift of the proton position toward $O_{(P1)}$. We did not observe any evidence that the second TMPO interfered through direct competition for the proton: the $O_{(P2)}$−H distance increased above 2.5 Å

DOI: 10.1021/acs.jpcc.6b03448
J. Phys. Chem. C 2016, 120, 19097−19106

Table 3. Relevant Interatomic Distances (Å) of the 2TMPO/1BA Configurations Shown in Figure 5a,b after Local Optimization

	internal BA	external BA
	Figure 5a[a]	Figure 5b
$O_{(P1)}$–H	1.016 (2.000)	1.033 (2.000)
$O_{(P2)}$–H	2.406 (2.000)	2.746 (2.000)
$O_{(P1)}$–$O_{(P2)}$	2.868 (2.462)	2.908 (2.462)
$O_{(Al)}$–H	1.635 (0.975)	1.541 (0.975)
$O_{(P1)}$–$O_{(Al)}$	2.547 (2.372)	2.544 (2.372)
P–$O_{(P1)}$	1.561	1.555
P–$O_{(P2)}$	1.504	1.499

[a]The values before the structural optimization are presented within parentheses.

during local optimization, which diminishes the possibility of H-bonding.

In contrast to the adsorption of a single TMPO molecule, where only strong acids are observed after both local optimization and MD, the systems composed of two TMPO molecules continued evolving during the MD simulation, modifying the acid strength classification given by the local optimization. At the internal surface, the movement of the TMPO molecules is capped owing to the reduced space inside the pore system. Therefore, we noticed a small shift of the protonated TMPO from $O1_{(Al)}$ to $O6_{(Al)}$, which was still enough to increase the separation from the second TMPO and establish a strong H-bond with $O6_{(Al)}$ (see Figure 6a and Table 4). As a consequence, the average $O_{(P1)}$–H bond length

Table 4. Relevant Interatomic Distances (Å) after 10 ps of MD Simulation Taking the 2TMPO/1BA Configurations Shown in Figure 5a,b as Input Geometries

	internal BA	external BA
	Figure 5a[a]	Figure 5b
$O_{(P1)}$–H	1.05 ± 0.04	1.07 ± 0.06
$O_{(P2)}$–H	5.0 ± 0.3	8.7 ± 0.2
$O_{(P1)}$–$O_{(P2)}$	4.7 ± 0.4	8.7 ± 0.2
$O_{(Al)}$–H	1.5 ± 0.1	1.5 ± 0.1
$O_{(P1)}$–$O_{(Al)}$	2.52 ± 0.09	2.5 ± 0.1
P–$O_{(P1)}$	1.57 ± 0.03	1.56 ± 0.02
P–$O_{(P2)}$	1.51 ± 0.02	1.52 ± 0.01

[a]Average and standard deviation over the last 2.5 ps of simulation.

increased to 1.05 Å after 10 ps of MD, from an initial value of 1.016 Å. The absence of confinement effects at the external surface allowed greater movement of the second TMPO, moving away from the first TMPO, to finally establish two strong H-bonds with nearby silanol groups (see Figure 6b). The withdrawal of the second TMPO from the vicinity of the protonated phosphine reduced the steric effects and hence enabled the reorientation of the first TMPO. Without steric interference, the acid proton could be better shared between the bridging $O1_{(Al)}$ and $O_{(P1)}$, which increased the $O_{(P1)}$–H bond length from 1.033 Å after local optimization to an average value of 1.07 Å after 10 ps of MD. Therefore, the very strong acidity predicted by the local relaxation was not conserved during the MD simulation; the BA site behaved as a strong acid instead.

3.3. Adsorption of Three TMPO Molecules. Proton transfer can be classified as weak for $O_{(P)}$–H distances that

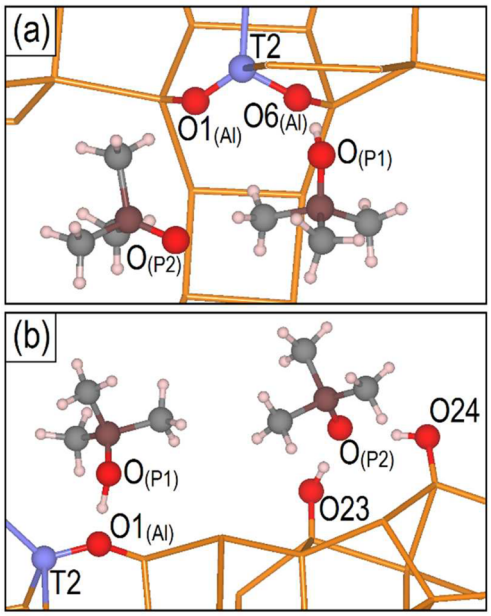

Figure 6. Representation of two TMPO molecules on (a) the internal BA site and (b) the external BA site after 10 ps of MD simulation of the locally optimized structure in Figure 5.

range from 1.097 to 1.188 Å (see Figure 2). We observed this weak acidity when a direct $O_{(P)}$–Al interaction was induced after adding a third phosphine oxide into the 2TMPO/1BA systems shown in Figure 5.

Figure 7 shows two equivalent structures after local optimization, out of several tested during our work, where $O_{(P1)}$–H bond lengths of 1.131 and 1.154 Å were obtained after adsorption on the internal and external surfaces, respectively; structural parameters of interest are compiled in Table 5. The proton was almost evenly shared between $O_{(Al)}$

Table 5. Relevant Interatomic Distances (Å) of the 3TMPO/1BA Configurations Shown in Figure 7a,b after Local Optimization

	internal BA	external BA
	Figure 7a[a]	Figure 7b
$O_{(P1)}$–H	1.131 (2.000)	1.154 (2.000)
$O_{(P2)}$–H	2.878 (2.000)	3.134 (2.000)
$O_{(P3)}$–H	3.125 (2.000)	3.599 (2.000)
$O_{(P1)}$–$O_{(P2)}$	3.548 (3.570)	4.034 (3.572)
$O_{(P1)}$–$O_{(P3)}$	3.473 (3.230)	4.144 (3.227)
$O_{(P2)}$–Al	1.993 (3.080)	2.033 (3.073)
$O_{(Al)}$–H	1.250 (0.975)	1.232 (0.975)
$O_{(P1)}$–$O_{(Al)}$	2.381 (2.627)	2.379 (2.627)
P–$O_{(P1)}$	1.533	1.531
P–$O_{(P2)}$	1.511	1.511
P–$O_{(P3)}$	1.501	1.496

[a]The values before the structural optimization are presented within parentheses.

and $O_{(P1)}$, rendering the acid response of the BA site weak. On this occasion, the average interaction energies for the internal and external BA sites differed by only 2 kJ/mol: −99 kJ/mol (internal) versus −97 kJ/mol (external). The adsorption at the internal surface, without considering the correction for dispersion forces, was repulsive, by 12 kJ/mol on average.

DOI: 10.1021/acs.jpcc.6b03448
J. Phys. Chem. C 2016, 120, 19097−19106

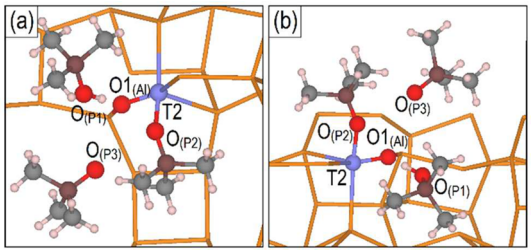

Figure 7. Representation of the adsorption of three TMPO molecules on (a) the internal and (b) the external BA sites after local optimization. H in white, C in gray, P in brown, O in red, Al in light blue, and Si represented by orange sticks. All the framework O atoms (except the protonated one) and silanol OH groups were deleted for an enhanced view. The interaction between one of the nonprotonated TMPO and the Al atom is represented by a stick connecting $O_{(P2)}$ to the Al atom. Related structural values are presented in Table 5.

Once the van der Waals interactions were taken into consideration, the overall adsorption energy became attractive, with a value of −99 kJ/mol. At the external surface, the dispersion contribution represented 77% of an average adsorption energy of −97 kJ/mol.

Our interpretation of the weakening of the acid as proton donor after the adsorption of three TMPO molecules was based on the strengthening of the $O_{(Al)}$−H bond. The $O_{(Al)}$−Al bond was weakened by the interaction between the Al atom and one of the nonprotonated TMPO molecules, which was reflected in $O_{(P)}$−Al distances that remained around 2.0 Å for both surfaces, as shown in Figure 7 and Table 5. There was also a large displacement of the Al atom during the optimization toward the nonprotonated phosphine. Under conditions of significant agglomeration of TMPO molecules around the BA site, the Al center may show residual Lewis acidity, with subsequent repercussions on the acid strength of the BA site. We did not observe direct competition for the acid proton by the nonprotonated phosphines, emphasized by $O_{(P2)}$−H and $O_{(P3)}$−H distances above 2.8 Å after local optimization.

In order to observe the perturbation and reordering of the electronic charge density derived from the TMPO-Al interaction, we have calculated the charge density difference for the configurations shown in Figure 7 according to the equation

$$\Delta\rho = \rho_{\text{zeolite+3TMPO}} - \rho_{\text{zeolite+2TMPO}} - \rho_{\text{1TMPO}} \quad (1)$$

The $\rho_{\text{zeolite+3TMPO}}$ term corresponds to the electronic density of the whole system with three TMPO molecules, while the density of the zeolite without the TMPO molecule closest to the Al atom is represented by the $\rho_{\text{zeolite+2TMPO}}$ term. The electronic density of the isolated phosphine oxide with exactly the same structure as when it was interacting with Al atom is denoted by the ρ_{1TMPO} term. We have used the same grid of points to represent the charge density and the same box size for the three calculations. The resulting distribution shows an increase of the charge density between $O_{(P2)}$ and Al atoms (see Figure 8), which highlights the formation of bonding interactions between both centers.

Figure 9 shows the projected density of states (PDOS) onto $O_{(P2)}(2p)$ of the TMPO interacting with the Al atom, as represented in Figure 7a, corresponding to the interior of the zeolite. The $O_{(P2)}(2p)$ PDOS presents intense peaks at the upper occupied edge of the energy spectra, between −2 and 0.0 eV (see Figure 9a). These $O_{(P)}(2p)$ states are complemented by small peaks in the Al(3s,3p) PDOS (Figure 9b,c) which disappear once the TMPO−Al interaction is deleted by removing the phosphine molecule (Figure 9d,e). In addition, the Al(3s,3p) PDOS reports the appearance of empty states above the Fermi energy as a result of the phosphine removal (Figure 9d,e). These transformations emphasize electron donation from the TMPO into empty electronic states associated with the Al atom.

After local optimization, there were differences in the behavior of the internal and external BA sites in the presence of three TMPO molecules. The internal ones almost always

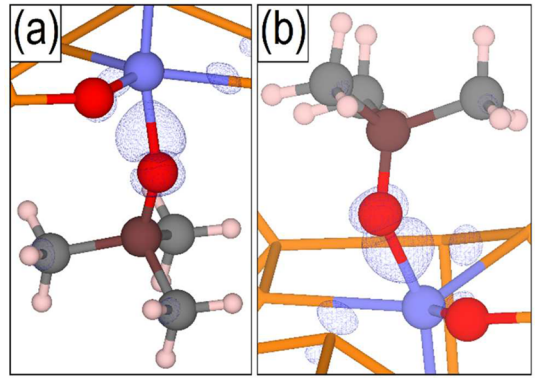

Figure 8. Charge difference isosurfaces with values of 0.005 $bohr^{-3}$ calculated from eq 1. (a) Internal BA site; (b) external BA site. The structures correspond to those shown in Figure 7. H in white, C in gray, P in brown, O in red, Al in light blue, and Si represented by orange sticks. All the framework O atoms (except the protonated one) and silanol OH groups were deleted for an enhanced view.

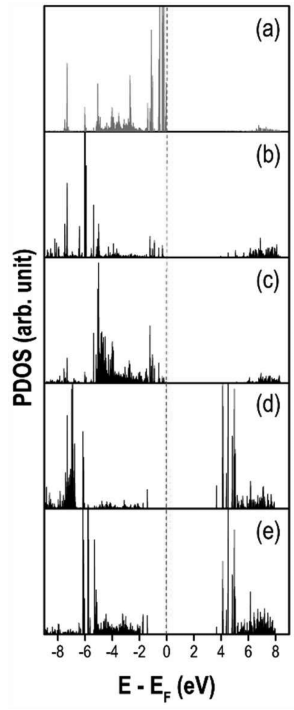

Figure 9. Projected density of states (PDOS) of (a) $O_{(P2)}(2p)$, (b) Al(3s), and (c) Al(3p) for the 3TMPO/1BA configuration observed in the cavity according to Figure 7a. PDOS of (d) Al(3s) and (e) Al(3p) for the structure without the nonprotonated TMPO that interacts with the Al center.

DOI: 10.1021/acs.jpcc.6b03448
J. Phys. Chem. C 2016, 120, 19097−19106

Table 6. Relevant Interatomic Distances (Å) for Six Different Configurations 3TMPO/1BA after Local Optimization

	internal BA configurations[a]			
	$O_{(P2)}$–Al	$O_{(Al)}$–Al	$O_{(P1)}$–H	acid class[c]
a	2.099	1.853	1.146	weak
b[b]	1.993	1.846	1.131	weak
c	2.149	1.839	1.107	weak
d	1.988	1.852	1.137	weak
e	2.245	1.822	1.093	strong
f	2.002	1.844	1.116	weak
	external BA configurations[a]			
	$O_{(P2)}$–Al	$O_{(Al)}$–Al	$O_{(P1)}$–H	acid class[c]
a	3.050	1.793	1.050	strong
b[b]	2.033	1.842	1.154	weak
c	5.554	1.812	1.053	strong
d	3.637	1.785	1.059	strong
e	3.059	1.789	1.047	strong
f	2.059	1.829	1.100	weak

[a]Second column: distance between $O_{(P2)}$ and Al in Figure 7. Third column: distance between $O_{(Al)}$ and Al. Fourth column: $O_{(P1)}$–H distance for the protonated TMPO in Figure 7. [b]Configurations shown in Figure 7 [c]Acid classification according to Figure 2.

performed as weak acids, whereas the external BA sites varied in strength between strong and weak, depending on the configuration; Table 6 summarizes these tendencies. When the $O_{(P2)}$ atom remained at less than 2.15 Å from the Al, the proton transfer was weak. Once this distance increased and the nonprotonated TMPO moved away from the Al atom, which was the case in four out of six configurations considered for the external BA site, the acidity was classified as strong. These findings underline the importance of the TMPO–Al interaction for the presence of the weak acidity.

The locally optimized arrangements of three TMPO molecules evolved differently during the MD simulation, depending on whether the adsorption took place at the internal or external surface. The MD calculations were performed on the configurations shown in Figure 7, with the average of the main structural parameters compiled in Table 7. The internal BA site continued to behave as a weak acid after 10 ps of dynamics, mostly due to the conservation of the initial configuration given as an input, with $O_{(P2)}$ atom binding the Al center. However, at the external surface the agglomeration of three TMPO molecules at the acid site was not preserved; both nonprotonated TMPO molecules moved away toward nearby silanol groups to establish H-bonds. Once the $O_{(P2)}$–Al link was broken, the acid strength of the external BA was again strong, illustrated by an average $O_{(P1)}$–H bond length of 1.05 Å. This exemplifies how equivalent BA sites are driven to behave differently as a consequence of the confinement produced by the pore system. The same confinement may be mimicked at the external surface if a large enough number of TMPO molecules is adsorbed in the vicinity of the BA site, limiting the movement of those phosphines that are in direct contact with the acid.

Table 7. Relevant Interatomic Distances (Å) after 10 ps of MD Simulation Taking the 3TMPO/1BA Configurations Shown in Figure 7a,b as Input Geometries

	internal BA	external BA
	Figure 7a[a]	Figure 7b
$O_{(P1)}$–H	1.2 ± 0.1	1.05 ± 0.05
$O_{(P2)}$–H	3.7 ± 0.2	6.5 ± 0.3
$O_{(P3)}$–H	5.6 ± 0.5	8.8 ± 0.5
$O_{(P1)}$–$O_{(P2)}$	4.9 ± 0.2	6.6 ± 0.3
$O_{(P1)}$–$O_{(P3)}$	6.3 ± 0.5	9.5 ± 0.5
$O_{(P2)}$–Al	2.0 ± 0.1	6.3 ± 0.2
$O_{(Al)}$–H	1.3 ± 0.2	1.5 ± 0.1
$O_{(P1)}$–$O_{(Al)}$	2.46 ± 0.09	2.52 ± 0.09
P–$O_{(P1)}$	1.55 ± 0.03	1.56 ± 0.02
P–$O_{(P2)}$	1.52 ± 0.02	1.53 ± 0.02
P–$O_{(P3)}$	1.50 ± 0.02	1.51 ± 0.03

[a]Average and standard deviation over the last 2.5 ps of simulation.

3.4. Full Deprotonation of the Brønsted Acid Site. We have considered the migration of a protonated TMPO from the vicinity of the BA site by moving the phosphine to the second pore interception that is present within the MFI unit cell. The distance between the acid proton and any of the four O atoms binding the Al center was larger than 5 Å before relaxation, rendering the acid site fully deprotonated. After local optimization, the $O_{(P)}$–H bond length decreased to 0.979 and 1.005 Å for adsorption at the internal and the external surfaces, respectively; Figure 10 shows the optimized geometries, with the O–H distances compiled in Table 8. Those bond lengths correspond to ^{31}P chemical shifts of around 86 ppm, which translates into an acid classification of very strong (see Figure 2). The framework O atoms that do not bind the Al center are not basic enough to lengthen the $O_{(P)}$–H bond, even if a H-bond is established. The MD simulation did not result in further modifications, with average $O_{(P)}$–H bond lengths remaining around 1.00 Å (see Table 8).

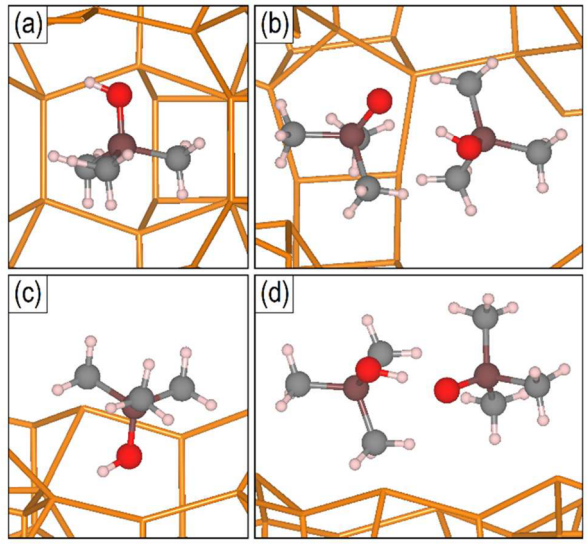

Figure 10. Representation of (a, c) $TMPOH^+$ and (b, d) $(TMPO)_2H^+$ at more than 5 Å away from the BA site after local optimization. (a, b) Internal surface; (c, d) external surface. H in white, C in gray, P in brown, O in red, and Si represented by orange sticks. All the framework O atoms (except the protonated one) and silanol OH groups were deleted for an enhanced view. Related structural values are presented in Table 8.

We also placed a second TMPO molecule in close proximity to the protonated phosphine in order to form the species $(TMPO)_2H^+$ and thus to induce the sharing of the acid proton

DOI: 10.1021/acs.jpcc.6b03448
J. Phys. Chem. C 2016, 120, 19097–19106

Table 8. Relevant Interatomic Distances (Å) of the Fully Protonated TMPO Molecules at More than 5 Å from the BA Site

	internal BA		external BA	
	$TMPOH^+$ (Figure 10a)	$(TMPO)_2H^+$ (Figure 10b)	$TMPOH^+$ (Figure 10c)	$(TMPO)_2H^+$ (Figure 10d)
	local optimization[a]			
$O_{(P1)}$–H	0.979	0.996	1.005	1.072
$O_{(P2)}$–H	–	2.167	–	1.431
P–$O_{(P1)}$	1.594	1.600	1.576	1.570
P–$O_{(P2)}$	–	1.515	–	1.522
$O_{(Si)}$–H	2.802	–	1.708	–
	MD simulation[b]			
$O_{(P1)}$–H	1.00 ± 0.04	1.11 ± 0.08	1.00 ± 0.02	1.2 ± 0.1
$O_{(P2)}$–H	–	1.4 ± 0.1	–	1.3 ± 0.1
P–$O_{(P1)}$	1.59 ± 0.04	1.57 ± 0.03	1.60 ± 0.05	1.55 ± 0.03
P–$O_{(P2)}$	–	1.53 ± 0.02	–	1.54 ± 0.03
$O_{(Si)}$–H	1.9 ± 0.4	–	2.3 ± 0.5	–

[a]Values after local optimization. The optimized structures are shown in Figure 10a–d. [b]Average values over the last 2.5 ps out of 10 ps of MD simulation taking the configurations shown in Figure 10a–d as input geometries.

between both molecules. After local optimization, the $O_{(P1)}$–H bond length at the interior of the zeolite remained 0.996 Å, corresponding to a very strong protonation. The equivalent value at the external surface increased to 1.072 Å, but still within the range of $O_{(P)}$–H distances sensed as a strong protonation by ^{31}P NMR. The second TMPO molecule had $O_{(P2)}$–H distances of 2.167 and 1.431 Å for the internal and external surfaces, respectively.

During the MD simulation the proton became more evenly shared between both TMPO molecules, increasing the average $O_{(P1)}$–H bond length to 1.1 or 1.2 Å and decreasing the $O_{(P2)}$–H distance to 1.4 or 1.3 Å depending on the surface (see Table 8); those values correspond to ^{31}P chemical shifts that classify the acid strength as weak. Therefore, full proton transfer may be probed experimentally as either very strong or weak, depending on whether the proton is binding a single TMPO or is shared between two phosphine molecules, respectively. During the adsorption of TMPO on Keggin-type 12-tungstophosphoric acid (HPW),[41] $TMPOH^+$ species appear within the region 95–85 ppm, while the formation of $(TMPO)_2H^+$ moves the ^{31}P chemical shift into the range 75–53 ppm, in agreement with our calculated $O_{(P)}$–H distances. However, the signals associated with $(TMPO)_2H^+$ disappear after thermal pretreatment of the sample, to emerge again when the sample is oversaturated with TMPO molecules.[41] Extrapolating to the zeolite MFI, it is more probable that the formation of $(TMPO)_2H^+$ occurs at the external surface, where the acid sites are exposed to higher loads of TMPO molecules than at the internal surface.

The implications of the $(TMPO)_2H^+$ formation depend on its coexistence with the other arrangements analyzed above. The acid proton may be shared between $O_{(P)}$ and $O_{(Al)}$, or between $O_{(P1)}$ and $O_{(P2)}$; the former alternative produces a strong proton transfer, as it was observed above after the MD simulation, while the latter corresponds to $(TMPO)_2H^+$, interpreted as weak acidity in the ^{31}P NMR spectrum. The relative occurrence of the first or the second alternative should depend on the number and mobility of TMPO molecules throughout the framework. For instance, a second TMPO can get close to the acid site where a protonated phosphine is already interacting through an H-bond with one of the $O_{(Al)}$ atoms. The second $O_{(P2)}$ may replace $O_{(Al)}$ within the H-bond to form $(TMPO)_2H^+$ (our MD simulation was too short to observe this transformation when more than one TMPO was adsorbed). Although $O_{(P2)}$ is more basic than $O_{(Al)}$, both TMPO molecules must have a specific orientation to properly share the proton. Owing to the presence of the $(CH_3)_3P$ segment, steric effects may play against the formation of $(TMPO)_2H^+$, which are accentuated by the confinement along the pore system. At the external surface, the TMPO's mobility and number increase as well as the access to the acid sites. This favors the formation of $(TMPO)_2H^+$ over the adsorption of a single TMPO at the acid site and may be the reason behind the disappearance of the ^{31}P signal for strong acids at the external surface of zeolite MFI.[10,12] Once the $(TMPO)_2H^+$ is formed, an additional equilibrium between $(TMPO)_2H^+$ and ($TMPOH^+$ + TMPO) can be established. This suggestion may explain the presence of very strong proton transfer, considering that we only observed an average $O_{(P)}$–H bond length below 1.01 Å after MD simulation for the $TMPOH^+$ species in Table 8. A similar process has been proposed for the solvation of H^+ ions in an aqueous medium, where an interconversion between $H_5O_2^+$ and (H_3O^+ + H_2O) is observed using Car–Parrinello MD.[35]

4. CONCLUSIONS

We have used DFT with dispersion corrections to study the adsorption of TMPO at the internal and external surfaces of zeolite MFI, with the T2-site substituted by Al. We initiated relaxation of the structures using local geometry optimization, followed by 10 ps of MD centered at 300 K; we considered the MD results as the final criterion to characterize the acid site. The acid should perform as strong, according to the ^{31}P chemical shift, when the proton is shared between the TMPO's oxygen atom and one of the framework O atoms that bind the Al. This trend holds when the number of TMPO molecules around the BA site increases, being the only exception the adsorption of three molecules at the internal surface. In that case, one of the nonprotonated TMPO molecules directly interacts with the Al center through direct contact between $O_{(P)}$ and Al. This interaction weakens the $O_{(Al)}$–Al bond, making the $O_{(Al)}$–H bond stronger and less prone to be broken; in consequence an $O_{(P)}$–H bond length of 1.2 Å is calculated, which translates into an acid strength classified as weak by ^{31}P NMR. The TMPO–Al interaction is more likely at the internal surface, where confinement effects keep the TMPO within close proximity of the Al atom. At the external surface, the nonprotonated TMPO molecules tend to migrate from the acid site, and establish H-bonds with nearby silanol groups.

We only observed $O_{(P)}$–H bond lengths smaller than 1.01 Å (acid classified as very strong by ^{31}P NMR) when a protonated TMPO was assumed to migrate from the acid site. In the absence of H-bonding between $O_{(P)}$ and $O_{(Al)}$, the $O_{(P)}$–H bond becomes shorter. Furthermore, if the acid proton is shared between two TMPO molecules, forming $(TMPO)_2H^+$, the $O_{(P)}$–H bond length increases to an average value between 1.1 and 1.2 Å, producing ^{31}P chemical shifts that classify the acid as weak. Therefore, the three main regions in the ^{31}P spectrum that are used to classify the acid sites as very strong

DOI: 10.1021/acs.jpcc.6b03448
J. Phys. Chem. C 2016, 120, 19097–19106

(90−80 ppm), strong (80−70 ppm), and weak (70−60 ppm) may be derived from the coexistence of the species $TMPOH^{+}\cdots O_{(Si)}$ (very strong), $TMPOH^{+}\cdots O_{(Al)}$ (strong), and $(TMPO)_2H^{+}$ (weak).

AUTHOR INFORMATION

Corresponding Author

*E-mail: deleeuwn@cardiff.ac.uk.

Notes

The authors declare no competing financial interest.

ACKNOWLEDGMENTS

The authors acknowledge the use of the UCL Legion High Performance Computing Facility (Legion@UCL), and associated support services, in the completion of this work. Via our membership of the UK's HEC Materials Chemistry Consortium, which is funded by EPSRC (EP/L000202), this work used the ARCHER UK National Supercomputing Service. This work was also performed using the computational facilities of the Advanced Research Computing@Cardiff (ARCCA) Division, Cardiff University. We acknowledge UCL and the UK Engineering and Physical Sciences Research Council (Grant EP/K009567/2) for funding. Nora H. de Leeuw thanks the Royal Society for an Industry Fellowship. All data created during this research is openly available from the University of Cardiff Research Portal at http://dx.doi.org/10.17035/d.2016.0009738222.

REFERENCES

(1) Sandoval-Díaz, L.-E.; González-Amaya, J.-A.; Trujillo, C.-A. General Aspects of Zeolite Acidity Characterization. *Microporous Mesoporous Mater.* **2015**, *215*, 229−243.

(2) Vermeiren, W.; Gilson, J.-P. Impact of Zeolites on the Petroleum and Petrochemical Industry. *Top. Catal.* **2009**, *52*, 1131−1161.

(3) Weitkamp, J. Zeolites and Catalysis. *Solid State Ionics* **2000**, *131*, 175−188.

(4) Moliner, M.; Martínez, C.; Corma, A. Multipore Zeolites: Synthesis and Catalytic Applications. *Angew. Chem., Int. Ed.* **2015**, *54*, 3560−3579.

(5) Čejka, J.; Wichterlová, B. Acid-Catalyzed Synthesis of Mono- and Dialkyl Benzenes Over Zeolites: Active Sites, Zeolite Topology, and Reaction Mechanisms. *Catal. Rev.: Sci. Eng.* **2002**, *44*, 375−421.

(6) Derouane, E. G.; Védrine, J. C.; Pinto, R. R.; Borges, P. M.; Costa, L.; Lemos, M. A. N. D. A.; Lemos, F.; Ribeiro, F. R. The Acidity of Zeolites: Concepts, Measurements and Relation to Catalysis: A Review on Experimental and Theoretical Methods for the Study of Zeolite Acidity. *Catal. Rev.: Sci. Eng.* **2013**, *55*, 454−515.

(7) Zheng, A.; Liu, S.-B.; Deng, F. Acidity Characterization of Heterogeneous Catalysts by Solid-State NMR Spectroscopy Using Probe Molecules. *Solid State Nucl. Magn. Reson.* **2013**, *55*−*56*, 12−27.

(8) Xu, J.; Zheng, A.; Yang, J.; Su, Y.; Wang, J.; Zeng, D.; Zhang, M.; Ye, C.; Deng, F. Acidity of Mesoporous MoOx/ZrO2 and WOx/ZrO2Materials: A Combined Solid-State NMR and Theoretical Calculation Study. *J. Phys. Chem. B* **2006**, *110*, 10662−10671.

(9) Li, S.; Huang, S.-J.; Shen, W.; Zhang, H.; Fang, H.; Zheng, A.; Liu, S.-B.; Deng, F. Probing the Spatial Proximities among Acid Sites in Dealuminated H-Y Zeolite by Solid-State NMR Spectroscopy. *J. Phys. Chem. C* **2008**, *112*, 14486−14494.

(10) Zhao, Q.; Chen, W.-H.; Huang, S.-J.; Wu, Y.-C.; Lee, H.-K.; Liu, S.-B. Discernment and Quantification of Internal and External Acid Sites on Zeolites. *J. Phys. Chem. B* **2002**, *106*, 4462−4469.

(11) Zheng, A.; Zhang, H.; Lu, X.; Liu, S.-B.; Deng, F. Theoretical Predictions of 31P NMR Chemical Shift Threshold of Trimethylphosphine Oxide Absorbed on Solid Acid Catalysts. *J. Phys. Chem. B* **2008**, *112*, 4496−4505.

(12) Seo, Y.; Cho, K.; Jung, Y.; Ryoo, R. Characterization of the Surface Acidity of MFI Zeolite Nanosheets by 31 P NMR of Adsorbed Phosphine Oxides and Catalytic Cracking of Decalin. *ACS Catal.* **2013**, *3*, 713−720.

(13) Ni, Y.; Sun, A.; Wu, X.; Hai, G.; Hu, J.; Li, T.; Li, G. The Preparation of Nano-Sized H[Zn,Al]ZSM-5 Zeolite and Its Application in the Aromatization of Methanol. *Microporous Mesoporous Mater.* **2011**, *143*, 435−442.

(14) Costa, C.; Dzikh, I. P.; Lopes, J. M.; Lemos, F.; Ribeiro, F. R. Activity−acidity Relationship in Zeolite ZSM-5. Application of Brönsted-Type Equations. *J. Mol. Catal. A: Chem.* **2000**, *154*, 193−201.

(15) Kwok, T. J.; Jayasuriya, K.; Damavarapu, R.; Brodman, B. W. Application of H-ZSM-5 Zeolite for Regioselective Mononitration of Toluene. *J. Org. Chem.* **1994**, *59*, 4939−4942.

(16) Wang, Y.; Jian, G.; Peng, Z.; Hu, J.; Wang, X.; Duan, W.; Liu, B. Preparation and Application of Ba/ZSM-5 Zeolite for Reaction of Methyl Vinyl Ether and Methanol. *Catal. Commun.* **2015**, *66*, 34−37.

(17) Zheng, A.; Han, B.; Li, B.; Liu, S.-B.; Deng, F. Enhancement of Brønsted Acidity in Zeolitic Catalysts due to an Intermolecular Solvent Effect in Confined Micropores. *Chem. Commun.* **2012**, *48*, 6936−6938.

(18) Kresse, G.; Hafner, J. Ab Initio Molecular Dynamics for Liquid Metals. *Phys. Rev. B: Condens. Matter Mater. Phys.* **1993**, *47*, 558−561.

(19) Kresse, G.; Hafner, J. Ab Initio Molecular-Dynamics Simulation of the Liquid-Metal−amorphous-Semiconductor Transition in Germanium. *Phys. Rev. B: Condens. Matter Mater. Phys.* **1994**, *49*, 14251−14269.

(20) Kresse, G.; Furthmüller, J. Efficiency of Ab-Initio Total Energy Calculations for Metals and Semiconductors Using a Plane-Wave Basis Set. *Comput. Mater. Sci.* **1996**, *6*, 15−50.

(21) Kresse, G.; Furthmüller, J. Efficient Iterative Schemes for Ab Initio Total-Energy Calculations Using a Plane-Wave Basis Set. *Phys. Rev. B: Condens. Matter Mater. Phys.* **1996**, *54*, 11169−11186.

(22) Perdew, J. P.; Burke, K.; Ernzerhof, M. Generalized Gradient Approximation Made Simple. *Phys. Rev. Lett.* **1996**, *77*, 3865−3868.

(23) Grimme, S. Semiempirical GGA-Type Density Functional Constructed with a Long-Range Dispersion Correction. *J. Comput. Chem.* **2006**, *27*, 1787−1799.

(24) Hernandez-Tamargo, C. E.; Roldan, A.; de Leeuw, N. H. A Density Functional Theory Study of the Structure of Pure-Silica and Aluminium-Substituted MFI Nanosheets. *J. Solid State Chem.* **2016**, *237*, 192−203.

(25) Blöchl, P. E. Projector Augmented-Wave Method. *Phys. Rev. B: Condens. Matter Mater. Phys.* **1994**, *50*, 17953−17979.

(26) Kresse, G.; Joubert, D. From Ultrasoft Pseudopotentials to the Projector Augmented-Wave Method. *Phys. Rev. B: Condens. Matter Mater. Phys.* **1999**, *59*, 1758−1775.

(27) Ho, K.-M.; Fu, C. L.; Harmon, B. N.; Weber, W.; Hamann, D. R. Vibrational Frequencies and Structural Properties of Transition Metals via Total-Energy Calculations. *Phys. Rev. Lett.* **1982**, *49*, 673−676.

(28) Fu, C.-L.; Ho, K.-M. First-Principles Calculation of the Equilibrium Ground-State Properties of Transition Metals: Applications to Nb and Mo. *Phys. Rev. B: Condens. Matter Mater. Phys.* **1983**, *28*, 5480−5486.

(29) Quartieri, S.; Arletti, R.; Vezzalini, G.; Di Renzo, F.; Dmitriev, V. Elastic Behavior of MFI-Type Zeolites: 3 − Compressibility of Silicalite and Mutinaite. *J. Solid State Chem.* **2012**, *191*, 201−212.

(30) Kokotailo, G. T.; Lawton, S. L.; Olson, D. H.; Meier, W. M. Structure of Synthetic Zeolite ZSM-5. *Nature* **1978**, *272*, 437−438.

(31) Nosé, S. A Unified Formulation of the Constant Temperature Molecular Dynamics Methods. *J. Chem. Phys.* **1984**, *81*, 511.

(32) Nosé, S. Constant Temperature Molecular Dynamics Methods. *Prog. Theor. Phys. Suppl.* **1991**, *103*, 1−46.

(33) Bylander, D. M.; Kleinman, L. Energy Fluctuations Induced by the Nosé Thermostat. *Phys. Rev. B: Condens. Matter Mater. Phys.* **1992**, *46*, 13756−13761.

(34) Momma, K.; Izumi, F. VESTA 3 for Three-Dimensional Visualization of Crystal, Volumetric and Morphology Data. *J. Appl. Crystallogr.* **2011**, *44*, 1272−1276.

DOI: 10.1021/acs.jpcc.6b03448
J. Phys. Chem. C 2016, 120, 19097−19106

(35) Tuckerman, M.; Laasonen, K.; Sprik, M.; Parrinello, M. Ab Initio Molecular Dynamics Simulation of the Solvation and Transport of Hydronium and Hydroxyl Ions in Water. *J. Chem. Phys.* **1995**, *103*, 150.
(36) Henkelman, G.; Arnaldsson, A.; Jónsson, H. A Fast and Robust Algorithm for Bader Decomposition of Charge Density. *Comput. Mater. Sci.* **2006**, *36*, 354−360.
(37) Sanville, E.; Kenny, S. D.; Smith, R.; Henkelman, G. Improved Grid-Based Algorithm for Bader Charge Allocation. *J. Comput. Chem.* **2007**, *28*, 899−908.
(38) Tang, W.; Sanville, E.; Henkelman, G. A Grid-Based Bader Analysis Algorithm without Lattice Bias. *J. Phys.: Condens. Matter* **2009**, *21*, 084204.
(39) Wernet, P.; Nordlund, D.; Bergmann, U.; Cavalleri, M.; Odelius, M.; Ogasawara, H.; Näslund, L. A.; Hirsch, T. K.; Ojamäe, L.; Glatzel, P.; et al. The Structure of the First Coordination Shell in Liquid Water. *Science* **2004**, *304*, 995−999.
(40) Ambrosetti, A.; Alfè, D.; Robert, A.; DiStasio, J.; Tkatchenko, A. Hard Numbers for Large Molecules: Toward Exact Energetics for Supramolecular Systems. *J. Phys. Chem. Lett.* **2014**, *5*, 849−855.
(41) Huang, S.-J.; Yang, C.-Y.; Zheng, A.; Feng, N.; Yu, N.; Wu, P.-H.; Chang, Y.-C.; Lin, Y.-C.; Deng, F.; Liu, S.-B. New Insights into Keggin-Type 12-Tungstophosphoric Acid from 31P MAS NMR Analysis of Absorbed Trimethylphosphine Oxide and DFT Calculations. *Chem. - Asian J.* **2011**, *6*, 137−148.

DOI: 10.1021/acs.jpcc.6b03448
J. Phys. Chem. C 2016, 120, 19097−19106